Available online at www.sciencedirect.com
SCIENCE DIRECT®
Journal of Nuclear Materials 350 (2006) 66–73
journal of nuclear materials
www.elsevier.com/locate/jnucmat

Interaction between borosilicate melt and Inconel

Pranesh Sengupta, J. Mittra, G.B. Kale *

Materials Science Division, Bhabha Atomic Research Centre, Mumbai 400 085, India

Received 25 July 2005; accepted 15 November 2005

Abstract

Understanding the mode of interaction between borosilicate melt and Inconel is important for long time usage of melter pot in vitrification plant. The present study shows that significant elemental exchanges take place across the borosilicate melt/Inconel interface resulting in the development of $(Fe, Ni)CrO_4$ needle and $(Fe, Ni)Cr_2O_4$ cubic phases. This results in significant depletion of Cr within Inconel near the interface. Beside these, CrB precipitates formed along the Inconel grain boundaries.

PACS: 28.41.Kw; 61.30.Ny; 05.70.Np

1. Introduction

Vitrification is most commonly used process for conditioning of high-level nuclear waste (HLW). It is an economical process and generates almost no secondary wastes. During the course of vitrification, organic matters and combustible materials associated with HLW get destroyed and the waste glass produced have adequate physical, mechanical and chemical durability required for nuclear waste form.

Preparation of waste glass is not as simple as making other commercial glasses. The major difference between the two is the radioactivity involved in the preparation of the former. A schematic diagram showing the HLW vitrification process is given in Fig. 1. There are several material related issues in this type of conditioning process. Among these, degradation of structural materials such as of melter pot during the course of waste glass generation demands significant attention. The major components of melter pot are schematically shown in Fig. 2(a). The complicated HLW chemistry and the procedure followed to condition the same produces extremely corrosive environment within the melter pot. Different components of the harsh environment that exist during vitrification process are shown schematically in Fig. 2(b). It is clear from this diagram that the material of construction of melter pot and its associated components like thermocouples, electrodes etc experience variable modes of degradation along their entire length during vitrification. Moreover, since plant scale vitrification is a batch process, it makes the nature of degradation even more complicated. For example, the portion of a melter pot that interacted with vapor in an earlier batch of operation may get exposed to borosilicate melt in later

* Corresponding author. Tel.: +91 22 2559 5062; fax: +91 22 2550 5239.
E-mail address: gbkale@apsara.barc.ernet.in (G.B. Kale).

0022-3115/$ - see front matter © 2005 Elsevier B.V. All rights reserved.
doi:10.1016/j.jnucmat.2005.11.012

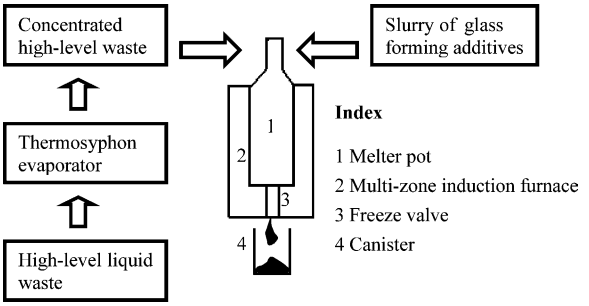

Fig. 1. Schematic diagram showing different stages of high-level waste vitrification process.

operations. Hence, reliable and repetitive large-scale operation in this regard is warranted by proper selection of materials for melter pot and other internal gadgets based on the knowledge of glass–alloy interaction and corrosion aspects.

Considering the harsh service environment involved in the vitrification process, nickel base alloy especially INCONEL® is regarded as a suitable melter pot material [1]. Rankin [2] and Bickford et al. [3] carried out extensive studies on these materials and identified certain Ni base alloys those have good resistance to aqueous, high temperature and molten salt corrosion; and also can withstand oxidizing environment (in general HLWs are concentrated nitric acid solution and thus build up oxidizing environment within melter pot during vitrification). Since presence of chromium gives better corrosion resistance to Ni-based alloys especially under oxidizing environment, so alloys like 690, 693 are commonly used as melter pot materials [1]. However, when vitrification is done purposefully under reducing environment (conditioning of sulfate rich HLWs in borosilicate glass matrix by adding charcoal [4]), alloy 625 (Inconel 625) may be tried as a melter pot material. Bulk composition of Inconel 625 is given in Table 1.

Several experiments have been carried out earlier to study the mode of interaction between Inconel and borosilicate/phosphate melt [1,5]. Many useful data are obtained on the corrosion of Inconel from such studies. But unfortunately nothing is known about the changes that take place within the waste glass melt after the interactions are over. This is largely because the experimental coupons (after putting inside the melt for certain time) were only studied in these experiments and the waste glass melt was either re-used for next set of experiments or discarded. To fill up this gap, the present experiments are so designed that waste glass compositions

Table 1
Composition of Inconel alloy 625

Element	wt%
Cr	22–23
Fe	5.0
Al	0.4
Mo	8–10
Ti	0.4
Si	0.5
Mn	0.5
P	0.015
C	0.10
Ni	Remaining

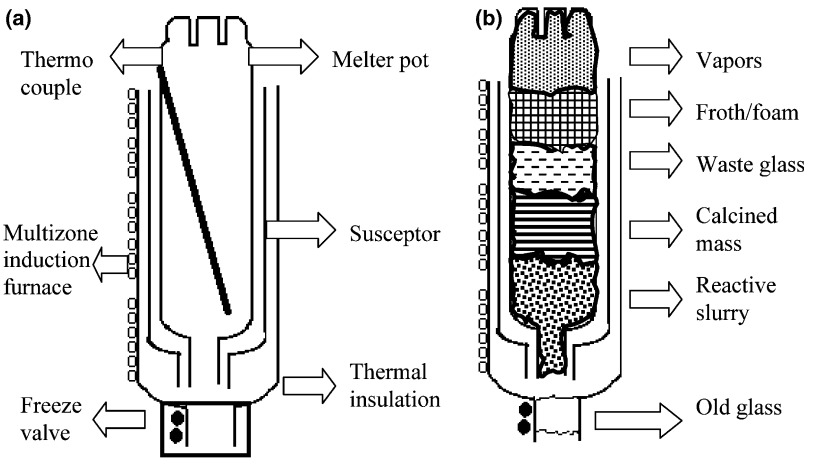

Fig. 2. Schematic diagrams showing (a) major components of melter pot and (b) different components of the harsh environment generated during vitrification process.

at the vicinity of Inconel coupon could also be studied. Results obtained from the present study are described below.

2. Experimental procedure

Experiments were carried out in two stages, (a) sample preparation and (b) chemical analysis of the same. The detailed descriptions of these stages are given below separately.

2.1. Sample preparation

Small cubical coupons of 10 mm × 10 mm × 10 mm dimensions were cut from Inconel (Alloy 625) plate. Each coupon was drilled at the centre to make small cylindrical cavity (~5 mm in diameter and ~5 mm in height). Inner walls of cavity were subsequently ground using abrasive rods and cleaned in ultrasonic bath.

Borosilicate melts used for the experiments were obtained by heating already prepared borosilicate waste glass at 1223 K. The waste glass was prepared through chemical route as indicated in Kaushik et al. [6]. A known amount of simulated waste was added with required amount of glass forming additives and the composition of the waste glass is given in Table 2. The mass was dried under infrared lamp, crushed to a fine powder and transferred to a fire clay crucible. The powder was heated in a step-wise thermal cycle and became pourable at 1223 K.

For the preparation of waste glass/Inconel couples, resistance furnace with argon atmosphere and temperature controller capable of maintaining temperature with ±1 K range was used. Freshly prepared borosilicate waste glass was broken into small pieces (0.5–2 mm) and put within the Inconel cavities. The filled coupons were then placed within the furnace and heated up in argon atmosphere. Each sample was held at 1223 K for time duration ranging from 28.8 ks to 345.60 ks allowing the Inconel coupon and waste glass melt to interact at that temperature. After the heat treatment, the samples were furnace cooled. All samples were cut vertically, along the axis of the cylindrical hole and the exposed surfaces were ground, polished and etched so as to reveal the microstructure of Inconel/waste glass interfaces.

Table 2
Borosilicate waste glass composition (in wt%)

Glass forming oxides	Simulated waste oxides
SiO_2: 35.50	FeO: 3.10
B_2O_3: 6.70	Na_2O: 3.40
Na_2O: 14.70	ZrO_2: 3.03
MnO: 9.60	MoO_3: 2.90
TiO_2: 6.50	RuO_2: 0.77
	Cs_2O: 1.54
	CeO_2: 4.80
	UO_2: 2.50
	Cr_2O_3, NiO, SrO, PdO, BaO, TeO_2: 3.76
	Sulfate: 1.20

Table 3
Crystals used for diffracting X-ray lines

X-ray line	Crystal	Name
Cu Kα	LIF	Lithium fluoride
Fe Kα, Cr Kα	PET	Penta erithrotol
Si Kα, Al Kα	TAP	Thallium acid pthalate
O Kα	PC1	Pseudocrystal 1
B Kα	PC3	Pseudocrystal 3

2.2. Chemical analysis

Interfacial characterizations of samples were done using Electron probe microanalyser (CAMECA SX 100). Polished metal/waste glass couples were coated with thin gold layer (~100 Å) for conductivity. An acceleration voltage of 20 keV and stabilized beam current of 4 nA and 20 nA were used for 'back scattered electron (BSE)' imaging and quantitative analysis respectively. The beam size was kept at ⩽1 μm to reduce the convolution effect so as to arrive at a better estimate of the phase compositions. Crystals used for diffracting different X-ray lines are given in Table 3. A program based on Pouchou and Pichoir (PAP) methods [7] was used for necessary atomic number (Z), absorption (A) and fluorescence (F) corrections so as to obtain true concentrations from the corresponding raw intensity data.

3. Results and discussion

3.1. Chemical changes within waste glass

Detailed EPMA study across the Inconel/waste glass interfaces indicated interesting physico-chemical changes within glass as well as within Inconel coupons. For each couple, Fig. 3(a) shows the BSE image of starting waste glass that is chemically homogeneous in nature. After thermal annealing for pre-determined time spans, waste glass portions adjacent to Inconel coupons became heterogeneous

in nature due to reaction between the two. This heterogeneous domain is henceforth mentioned as 'reaction zone'. The reaction zone developed at the interface for the sample annealed for 172 800 s is shown in Fig. 3(b). It is observed that the reaction zone is defined by the presence of needle and cubic shaped phases. The width of the reaction zone increased with the increase in time (Table 4). It is known that layer growth kinetics follow a non-linear relation

$$x = kt^{1/n},$$

where x is the reaction zone width, k is the reaction constant, t is time and n is reaction index. A binary plot of $\ln x$ vs $\ln t$ obtained from the present experiments is shown in Fig. 4 and the numerical value of 'n' calculated from slope of the best fitted straight line is 1.28. This value indicates that the reaction zones developed due to elemental diffusion in liquid state.

X-ray line scans taken across the Inconel/waste glass interface for the sample annealed for 18 000 s are shown in Fig. 5(a)–(e). It is observed that the reaction zone within the waste glass is compositionally defined by changes in Cr Kα profile (Fig. 5(a)). Within the reaction zone Cr Kα profile shows two peaks corresponding to cubic and needle phases, respectively.

Table 4
Time dependence of reaction zone width

Time (s)	1800	18 000	86 400	172 800
Width (μm)	4	8	10	17

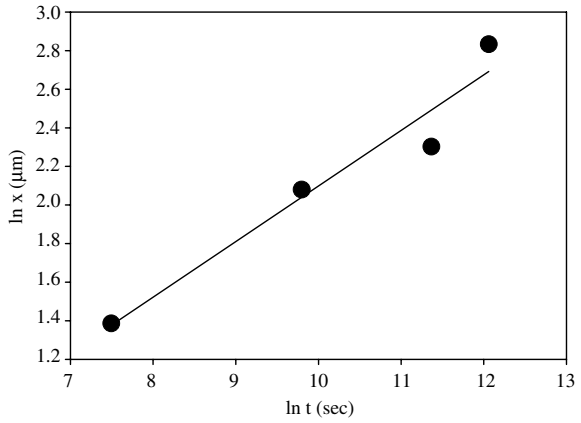

Fig. 4. Time (t) dependence of reaction zone width (x) growth.

Quantitative analyses have been carried out for the phases present in reaction zones. Due to small sizes of the phases accurate compositional data were difficult to obtain. For this reason, identification of

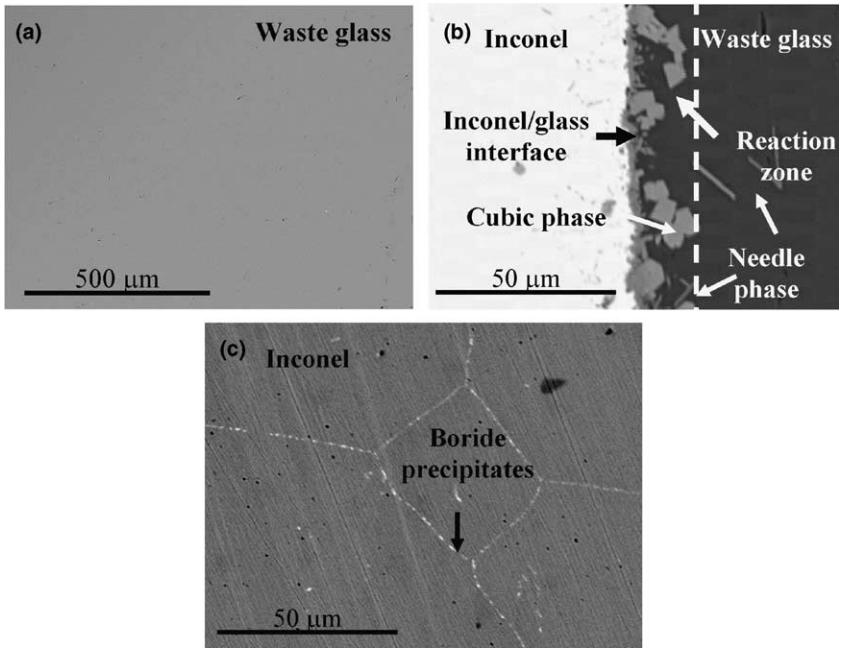

Fig. 3. BSE images showing (a) homogeneous nature of the starting waste glass, (b) development of reaction zone containing cubic and needle phases at the Inconel/waste glass interface of the sample annealed for 172 800 s and (c) presence of boride precipitates along the Inconel grain boundaries of the same sample.

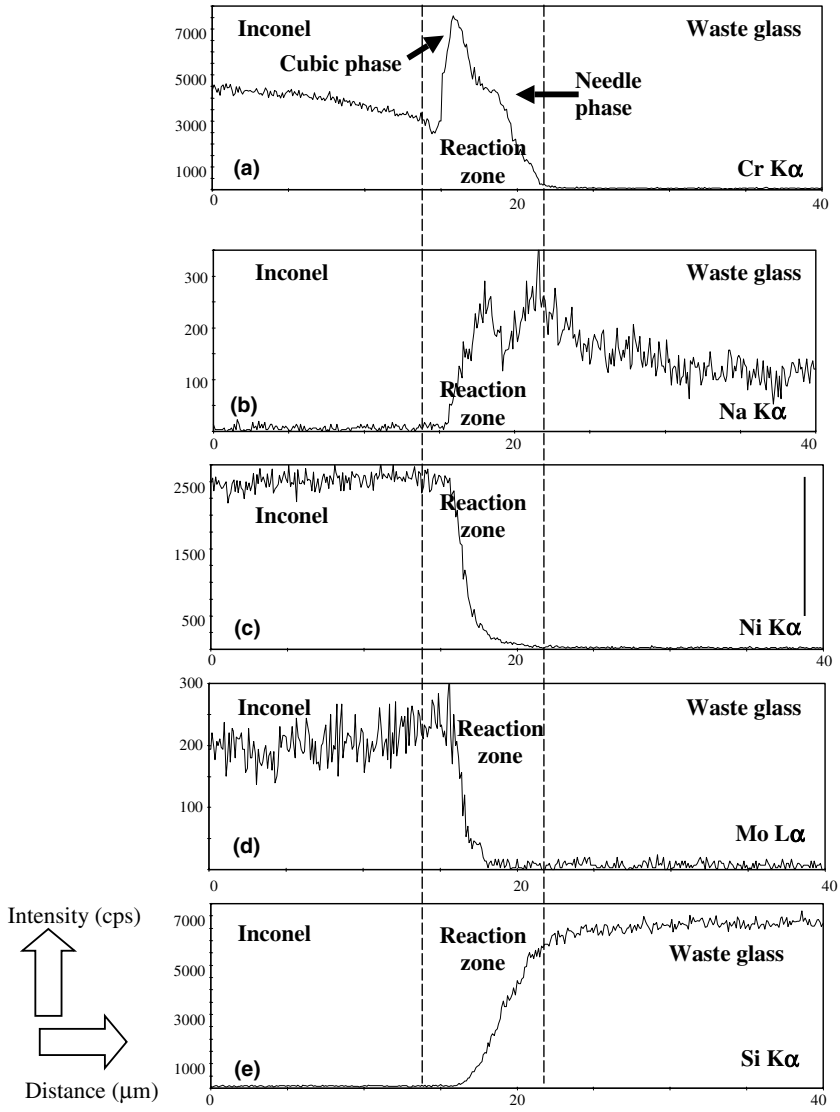

Fig. 5. X-ray line profiles for (a) Cr Kα, (b) Na Kα, (c) Ni Kα, (d) Mo Lα and (e) Si Kα taken across the Inconel/waste glass interface of the sample annealed for 18000 s.

phases has been done by combining EPMA data with relevant information collected from phase diagrams and crystallographic data. Based on this, the needle shaped phase is identified to be of (Fe, Ni)CrO_4 stoichiometry (Table 5). Crystallographically (Fe, Ni)CrO_4 belongs to orthorhombic system and hence it appear as needles adjacent to interface (Fig. 3(b)). Similarly, the cubic shaped phase is identified as spinel of (Fe, Ni)Cr_2O_4 stoichiometry (Table 5). Occurrence of $NiCrO_4$ and $NiCr_2O_4$ in $NiO–Cr_2O_3–O_2$ system has been reported by Muller et al. [8]. Presence of Fe within (Fe, Ni)Cr_2O_4 composition can be justified by the existence of solid solution between $NiCr_2O_4$ and $NiFe_2O_4$ spinels [9].

Table 5
Phases at the Inconel/waste glass interface

Composition (at.%)	Needle (Fe, Ni)CrO_4	Cubic (Fe, Ni)Cr_2O_4
Cr	13.42	27.32
Fe	2.06	10.05
Ni	12.67	5.80
Mo	1.32	–
Al	0.79	–
Ti	1.07	–
Si	2.11	–
O	Balance	56.83

Beside the formation of Cr rich phases, enrichment of Na along the interfaces is another

interesting aspect noted in the present study (Fig. 5(b)). Similar local enrichment in Na concentration at the interface has been reported by us earlier also [10]. Such local build up in Na concentration is of concern, especially for vitrification of sulphate rich HLW. It is known that during vitrification of such HLW, sulphate anions club with Na to form Na_2SO_4 (thenardite) rich clusters. This is commonly known as 'yellow phase' or 'gall' and it mostly occurs as froth within the melter. Development of sulfate rich froth within melter pot has two serious consequences. Firstly, it locally causes sulfur corrosion attack on the material. Secondly, it acts as a sink for ^{137}Cs and ^{90}Sr radionuclides present in the waste glass melt. Experiments are currently being carried out in laboratory to see the mode of corrosion of Inconel with yellow phase and sulfate vapors and the results will be reported some where else.

As shown in Fig. 3(b), $(Fe,Ni)CrO_4$ and $(Fe,Ni)Cr_2O_4$ phases are distributed within the waste glass matrix. X-ray intensity counts for major elements such as Si, B etc have been measured for the waste glass portions adjacent to the above phases and compared with those data obtained for precursor waste glass. It is observed that there are no significant variations in corresponding intensity values. The slope observed in the Si Kα profile (Fig. 5(e)) towards Inconel is thus due to presence of Si free cubic and needle phases within the reaction zone.

3.2. Chemical changes within Inconel

Changes within Inconel coupons due to interaction with waste glass melt have been documented in literature. Earlier, Vidensky et al. [5] studied the interactions between borosilicate melt with various Ni–Cr alloys including alloys 690 and 693 and recently Zhu et al. [1] carried out similar study between phosphate melt and alloys 690 and 693. They reported the development of $(Fe,Cr)_2O_3$ on material surfaces after corrosion. But in the present study we do not observe the formation of $(Fe,Cr)_2O_3$ although presence of $(Fe,Ni)Cr_2O_4$ spinel in waste glass is seen. Formation of $(Fe,Cr)_2O_3$ spinel in phosphate melt and alloy 690 could be due to higher content of Fe (9 wt%) in alloy and phosphate melt (20 wt%) compared to our Inconel (5 wt%) and borosilicate melt (~3 wt%). As seen from Cr Kα profile (Fig. 5(a)) it is clear that Inconel gets depleted in Cr near the interface. This compositional change of Inconel has been quantified and the values for the sample annealed for 86400 s are tabulated in Table 6. It is seen that an exposure of Inconel coupons to borosilicate melt for 86400 ks causes a depletion of ~6 wt% of Cr in Inconel compared to its original composition. Such significant depletion of Cr adjacent to interface is alarming as Cr offers resistance to intragranular and intergranular stress corrosion cracking attacks in Ni-base alloys [11].

Beside Cr, interesting results are obtained for Ni and Mo also. The intensities of Ni Kα and Mo Lα are observed to increase near the interface (Fig. 5(c) and (d)). This could be due to depletion of Cr in this region. Similar depletion of Cr and enrichment of Ni near waste glass/alloy 690 interfaces has been reported by Mirschinka et al. [12] also.

Another interesting aspect that has been noted in the present study is boride precipitation along the Inconel grain boundaries adjacent to Inconel/waste glass interfaces (Fig. 3(c)). It is to be noted here that the borides precipitates described here differ from those reported in alloy 718 on the basis of origin [13]. In alloy 718, borides are distributed along the grain boundaries and their source is the alloy itself. In the present case the precipitates along grain boundaries are seen only in region near Inconel/waste glass interface and the source of B is borosilicate melt. For detailed analysis of boride precipitates, Inconel coupon was allowed to interact with boric acid (powder) at 1223 K for 24 h in a separate experiment. After the annealing coarse boride precipitates formed along the grain boundaries and are shown in Fig. 6(a). X-ray line scans taken across the precipitates showed enrichment of Cr and B (Fig. 6(b)–(c)). Representative quantitative analysis of these precipitates is given in Table 7 and is

Table 6
Variations in Inconel alloy compositions near the interface for the sample annealed for 86400 s

Composition (wt%)	Cr	Fe	Ni	Mo	Al	Ti	Si
Away from interface	23.00	1.41	65.58	9.59	0.22	0.08	0.14
At interface	16.78	1.96	68.95	11.96	0.06	0.10	0.19

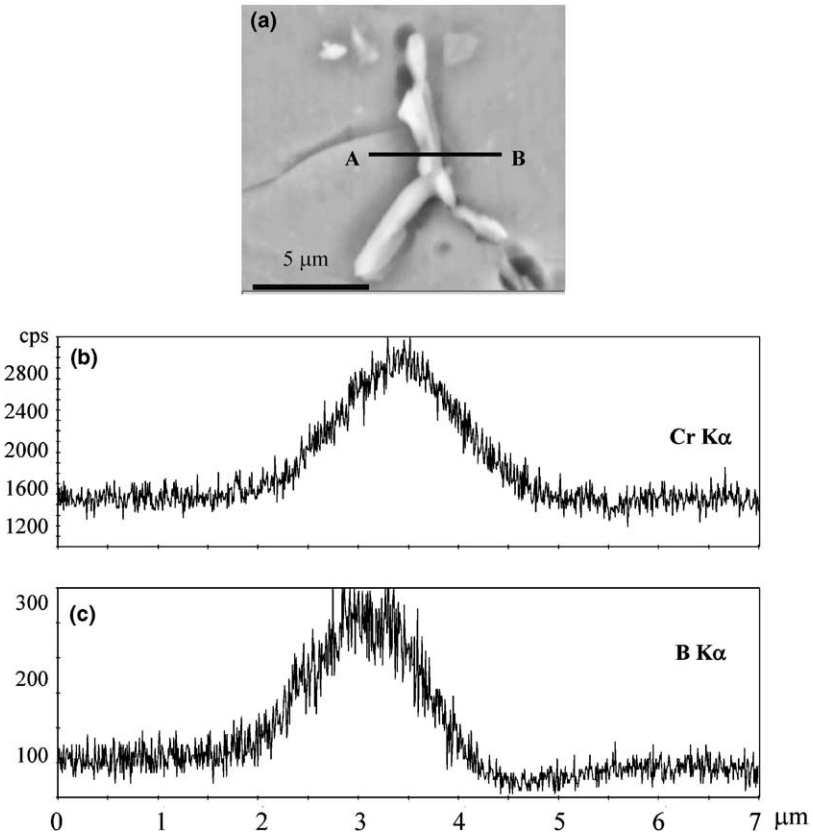

Fig. 6. A–B marker on (a) BSE image indicates the line along which, line profiles for (b) Cr Kα and (c) B Kα X-rays were taken (the sample was annealed for 172 800 s).

Table 7
Composition of boride precipitates

Element	B	Cr	Ni
Composition (at.%)	36.06	54.13	9.81

identified as CrB. As the precipitate is very thin Ni signal from substrate is also observed.

4. Conclusion

'Selection of material' for melter pot and associated gadgets is still being pursued by material scientists across the world. The present study shows significant elemental exchanges take place across the Inconel/borosilicate melt interfaces during vitrification. Ni and Cr diffuses from Inconel to borosilicate melt, causing development of $(Fe, Ni)CrO_4$ and $(Fe, Ni)Cr_2O_4$ phases within the melt at the interface. Formation of these oxide phases in abundance is a matter of concern from vitrification plant operation point of view. $(Fe, Ni)CrO_4$ and $(Fe, Ni)Cr_2O_4$ phases being of high density are likely to settle down in the melter pot during vitrification, and can cause clogging of freeze valve. Beside this, enrichment of sodium within borosilicate melt at the interface is another matter of serious concern (discussed before). Interestingly it is observed that Mo of Inconel gets retained within Inconel. This is beneficial, since Mo is also known to stabilize yellow phase in borosilicate melt [14].

Significant chromium depletion of the pot material at the interface is a very important aspect. Depletion of Cr can cause severe blistering at the metal surface [12] and hence can degrade the metallurgical properties of Inconel melter pot significantly. Effect of CrB precipitation along the Inconel grain boundaries on its metallurgical properties needs to be studied.

Finally it should be mentioned here that the present study gives an account how the precursor materials properties may change due to interaction between borosilicate melt and melter pot material. But this is only a small part of the effects that melter

pot material experiences during a single cycle of vitrification. As described by Vidensky et al. [5] alloy 690 suffers maximum degradation upon exposure to vapors compared to exposure to molten salt and glass melt. Further Gan et al. [15] showed corrosion of alloy 690 also depends on various other factors such as alternating current (AC) current density, melt compositions, temperature, and electrical waveform. In plant scale, the corrosion of melter pot material may become even more complicated due to periodic operation of vitrification cycles. Recently Iverson et al. [16] studied alloy 690 materials collected from a vitrification plant of Defence Waste Processing Facility, DOE (USA) that experienced a continuous service life of 8 years. They observed that the corrosion of alloy 690 components was no more severe than predicted by pilot scale melter and laboratory experience.

Acknowledgements

The authors are grateful to Dr S. Banerjee, Director, BARC, Mr B.P. Sharma, Associate Director, Materials Group and Head, Materials Science Division, BARC for their keen interest in the work.

References

[1] D. Zhu, C.W. Kim, D.E. Day, J. Nucl. Mater. 336 (2005) 47.
[2] W.N. Rankin, Adv. Ceram. 8 (1985) 559.
[3] D.F. Bickford, R.S. Ondrejcin, L. Salley, in: Proceedings Third International Symposium on Ceramics in Nuclear Waste Management II, American Ceramics Society, Chicago, 1986.
[4] T.P. Vasala, A. Joseph, R.G. Yeotikar, in: Proceedings Nuclear and Radiochemistry Symposium, Bhabha Atomic Research Centre, Mumbai, 2001, p. 542.
[5] I. Vidensky, H. Gan, I.L. Pegg, in: G.L. Smith, S.K. Sundaram, D.R. Spearing (Eds.), Environmental Issues and Waste Management Technologies, American Ceramic Society, 2004.
[6] C.P. Kaushik, R.K. Mishra, V.G. Katarni, A. Kumar, V. Thorat, N. Soudamini, P.D. Ozarde, K. Raj, P. Sengupta, G.B. Kale, P.K. De, in: BARC Reports, BARC/2004/E/019, 2004, p. 29.
[7] J.L. Pouchou, F. Pichoir, Microbeam Analysis, San Francisco, California, 1985, p. 104.
[8] O. Muller, R. Roy, W.B. White, J. Amer. Ceram. Soc. 51 (1968) 693.
[9] B.H. Park, D.S. Kim, Bull. Kor. Chem. Soc. 20 (1999) 939.
[10] V. Kain, P. Sengupta, P.K. De, S. Banerjee, Metall. Trans. A 36 (2005) 1075.
[11] H. Sahlaoui, H. Sidhom, J. Philbert, Acta Mater. 50 (2002) 1383.
[12] V. Mirschinka, S. Halazovich, R. Odoj, Mater. Res. Soc. Symp. Proc. 15 (1983) 695.
[13] W. Chen, M.C. Chaturvedi, N.L. Richards, G. McMohon, Metall. Trans. A 20 (1997) 1998.
[14] E. Schiewer, H. Rabe, S. Weisenburger, in: Sci. Basis for Radio. Waste Mgt. V, 1982, p. 289.
[15] H. Gan, A.C. Buechele, C.W. Kim, X. Huang, R.K. Mohr, I.L. Pegg, Mater. Res. Soc. Symp. Proc. 556 (1998) 278.
[16] D.C. Iverson, K.J. Imrich, D.F. Bickford, J.T. Gee, C.F. Jenkins, F.M. Heckendorn, in: J.D. Vienna, D.R. Spearing (Eds.), Environmental Issues and Waste Management Technologies IX, American Ceramic Society, 2004.